ACS APPLIED POLYMER MATERIALS

pubs.acs.org/acsapm Article

Multiscale Characterization of Thermoresponsive Poly(*N*-vinylcaprolactam) Across Hydration States for Drug Delivery

Camilla Hald Gregersen, Kārlis Bērziņš, Jacob Judas Kain Kirkensgaard, Işık Perçin Demirçelik, Charalampos Sideris, Ben J. Boyd, Jørn Bolstad Christensen, Andrea Heinz, and Hanne Mørck Nielsen*

Cite This: https://doi.org/10.1021/acsapm.6c02142 Read Online

ACCESS | Metrics & More | Article Recommendations | Supporting Information

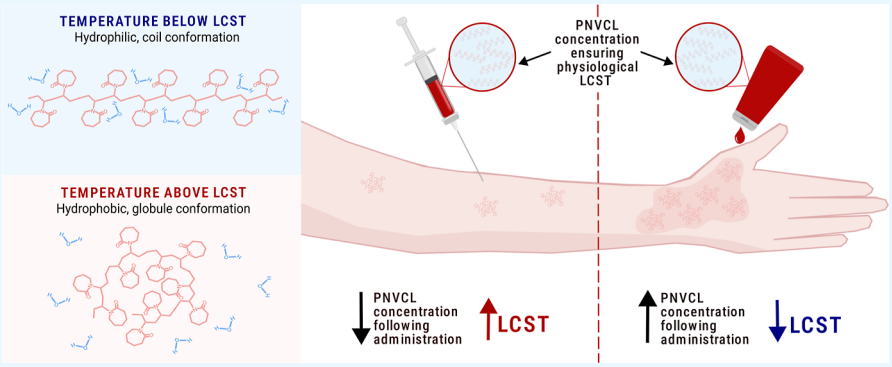

ABSTRACT: Poly(*N*-vinylcaprolactam) (PNVCL) is a thermoresponsive polymer of particular interest for stimuli-responsive drug delivery due to its physiologically relevant lower critical solution temperature (LCST). However, temperature-induced conformational changes vary significantly with polymer concentration, making the polymer's hydration state a crucial design parameter. In this study, we investigated the thermoresponsive properties of PNVCL at hydration states representative of various drug delivery applications, extending current knowledge on dissolved PNVCL to hydration states also relevant for cutaneous application. PNVCL with low molecular weight (<5000 g/mol) and low dispersity (1.2−1.8) was synthesized via free radical polymerization, and the molecular weight was characterized using a multimethod approach. UV−vis spectrophotometry, Raman spectroscopy, and small- and wide-angle X-ray scattering (SAXS/WAXS) were employed to probe conformational changes at multiple length scales. We found distinct structural transitions around the LCST for all hydration states, consistent with a coil-to-globule transition. The LCST exhibited a significant dependence on hydration state, with transitions occurring at 27 °C for powder PNVCL and at 48 °C for highly diluted PNVCL (10 mg/mL in water). These findings highlight the importance of accounting for concentration-dependent shifts in LCST when designing PNVCL-based drug delivery systems, particularly for applications involving changes in local polymer concentration upon administration.

KEYWORDS: *free radical polymerization, film-forming polymer, lower critical solution temperature, molecular weight characterization, Raman spectroscopy, small- and wide-angle X-ray scattering*

1. INTRODUCTION

Stimuli-responsive polymers represent a class of polymers that undergo significant changes in their physicochemical properties in response to subtle variations in stimuli. These include externally applied stimuli such as light, electric or magnetic fields, and physiological stimuli such as temperature, pH, or glucose levels.[1] Drug delivery systems employing stimuli-responsive materials have gained significant interest for triggering drug release in response to certain disease-specific physiological stimuli. Such tailored drug release can control drug absorption kinetics upon administration and reduce side effects by minimizing the nonspecific release of drugs when the triggering condition is not present.[1] In particular, thermoresponsive polymers are exploited due to spikes in body temperature as a vital physiological factor manifested in various diseases.[2] An example is the delivery of doxorubicin to tumor sites using the thermoresponsive polymer poly(*N*-isopropylacrylamide) (PNIPAM). At normal body temperature, doxorubicin is retained by PNIPAM, while the slight temperature increase at tumor sites serves as a trigger for drug release from the nanoparticles.[3]

Received: May 20, 2026
Revised: July 17, 2026
Accepted: July 21, 2026

A stimuli-responsive polymer that has recently gained focus for its potential in biomedical applications is poly(*N*-vinylcaprolactam) (PNVCL). So far, PNVCL has been used commercially in hair care products[4] and in the oil industry.[5] Yet, it holds several attributes that make it an ideal candidate for stimuli-responsive drug delivery. PNVCL is thermoresponsive with a lower critical solution temperature (LCST) tunable within the range of physiologically relevant temperatures, spanning from 32 to 50 °C.[6] In aqueous media, PNVCL exists in a hydrophilic, extended state below the LCST, but transitions into a hydrophobic, collapsed state above the LCST, undergoing a coil-to-globule conformational transition triggered by changes in temperature.[7,8] The importance of controlling molecular weight and dispersity through synthesis arises from PNVCL following Type 1 Flory−Huggins demixing behavior, which states that increased molecular weights result in decreased LCSTs.[7] This molecular weight dependence of the LCST is well reported in several experimental studies.[9,10] This behavior is opposite to that of PNIPAM, which exhibits an LCST that is nearly independent of molecular weight.[7] Other factors known to affect the LCST of PNVCL are polymer concentration, solvent, salt concentration, and copolymerization.[6,7,10,11] As an example, Marsili et al.[10] showed that when PNVCL-COOH was in contact with human plasma, the LCST decreased by as much as 10 °C. Structurally, PNVCL is a nonionic, amphiphilic polymer, characterized by a hydrophobic vinyl backbone and repeat units of hydrophilic amide groups, with the nitrogen atom of the amide group directly attached to the backbone. This structure makes PNVCL highly stable against hydrolysis at physiological conditions, suggesting a high biocompatibility.[12] PNVCL is nonbiodegradable, but in vitro cytotoxicity studies suggest high tolerability compared to PNIPAM. Vihola et al.[13] studied toxicity of PNVCL and PNIPAM in Caco-2 and Calu-3 cell lines and found no toxicity of PNVCL at all tested polymer concentrations (0.1−10 mg/mL) after 3 h incubation. After 12 h incubation, PNVCL showed a slight decrease in variability above its LCST, but still far less than that induced by PNIPAM.[13] In addition, PNVCL displays good solubility in both polar and nonpolar solvents, with a solubility in water up to 400 mg/mL, thus allowing versatile drug delivery applications.[6] The film-forming properties of PNVCL[4] and its demonstrated tolerability in skin cells (929L mouse fibroblasts)[14] make it particularly relevant for cutaneous application. These characteristics may help address unmet needs in cutaneous drug delivery by prolonging skin residence time through film formation while maintaining biocompatibility during extended exposure and simultaneously drive stimuli-responsive drug release to the skin triggered by skin temperature.[15] PNVCL has previously been investigated in various cutaneous applications, including fibers,[14,16,17] hydrogels,[18,19] deep eutectic solvents,[20] transdermal patches,[21] and hydrogel-forming microneedles.[22]

Free radical polymerization is a commonly used method for synthesizing PNVCL in a wide range of molecular weights, controlled through the monomer/initiator ratio[10] or incorporation of chain transfer agents.[9] Despite the current understanding of molecular weight control during polymerization, standardized and reproducible methods for free radical polymerization are limited in PNVCL literature, and control of molecular weight and dispersity remains a challenge.[6,7]

Current literature has demonstrated that even subtle variations in PNVCL concentration introduce variations in the LCST of several degrees, from below to above physiologically relevant temperatures.[6] When utilizing PNVCL for stimuli-responsive drug delivery that relies on body temperature as the trigger, this pronounced concentration dependence of the LCST must be carefully considered when selecting the administration route and dosage form. At the high polymer concentration associated with cutaneous application, the LCST is reduced, which may be exploited to enable the use of lower molecular weight PNVCL that otherwise exhibit higher intrinsic LCST values. On the other hand, administration routes involving dilution upon administration, such as injection, are expected to shift the LCST from body temperature to substantially higher temperature, thereby compromising temperature-triggered drug release under in vivo conditions.

Despite its clear relevance, the distinction between preadministration and postadministration concentration has received limited attention in the PNVCL literature. Existing studies on PNVCL have mainly focused on characterizing the thermoresponsive properties of PNVCL in solution.[9,10,17,19] In this work, we aimed to characterize the thermoresponsive properties of PNVCL under conditions that more closely mimic realistic application scenarios, such as in powder form and in a slightly hydrated state relevant for cutaneous application of PNVCL-based formulations. Furthermore, we aimed to address the potential implications that arise as a consequence of concentration changes resulting from PNVCL administration.

2. MATERIALS AND METHODS

2.1. Materials

N-vinylcaprolactam (NVCL) (purity ≥98% stabilized with 4-hydroxy-2,2,6,6-tetramethylpiperidine-1-oxyl (HO-TEMPO)) was purchased from Tokyo Chemical Industry (Tokyo, Japan). 1,4-dioxane, hexane (purity ≥95%), 2,2-azobis(isobutyronitrile) (AIBN) (purity ≥98%), and chloroform-D1 ($CDCl_3$) (purity 99.8%) were purchased from Merck (Darmstadt, Germany). Aluminum oxide was purchased from Thermo Fisher Scientific Inc. (Kandel, Germany). Super-DHB (a 9:1 mixture of 2,5-dihydroxybenzoic acid (DHB) and 2-hydroxy-5-methoxybenzoic acid), dichloromethane (DCM), and sodium trifluoroacetate (NaTFA) were purchased from Sigma-Aldrich (Søborg, Denmark). *N*,*N*-dimethylformamide (DMF) was purchased from VWR International (Leuven, Belgium). Ultrapure water (resistivity of 18.2 MΩ × cm) was obtained from a PURELAB flex 4 system (ELGA, LabWater, High Wycombe, UK). For comparison with synthesized PNVCL, commercially available PNVCL (Product ID P4364B-NVCL, viscosity-average molecular weight (M_v) = 1800 g/mol) was purchased from Polymer Source Inc. (Dorval, QC, Canada).

2.2. Synthesis and Purification of PNVCL

PNVCL was synthesized from NVCL by free radical polymerization. The purification process comprised evaporation of 1,4-dioxane, dialysis, and freeze-drying. The method was adapted from a previously published method by Medeiros et al.,[9] with several modifications of the synthesis and purification introduced through a range of optimization experiments. The optimization experiments aimed to achieve complete monomer conversion and efficient solvent removal through optimization of synthesis duration, rotary evaporation duration, and dialysis duration.

2.2.1. Free Radical Polymerization. Free radical polymerization components were AIBN (initiator), NVCL (monomer), and 1,4-dioxane (solvent). Prior to use, NVCL was recrystallized from hexane by dissolving 1 g/mL in a glass beaker under constant stirring at 40 °C. The NVCL precipitate was achieved by cooling the crystals for 10 min in an ice bath followed by heating for 10 s in a water bath of 70

https://doi.org/10.1021/acsapm.6c02142
ACS Appl. Polym. Mater. XXXX, XXX, XXX−XXX

°C, to just loosen the crystals from the glass beaker. The resulting mixture was poured through a Büchner funnel with filter paper (MN 615, Macherey-Nagel, Düren, Germany) to collect the NVCL, followed by overnight rotary evaporation to remove residual hexane. Immediately before starting the synthesis, 1,4-dioxane was passed through aluminum oxide in a filter funnel (pore size 10−16 μm, BRAND®, Wertheim, Germany) to remove reactive peroxides. For free radical polymerization, NVCL was transferred to the reactor along with 75% of the 1,4-dioxane volume and the mixture was flushed with nitrogen for 10 min while heating to 70 °C in a paraffin oil bath. A solution of AIBN and 25% of the 1,4-dioxane was prepared and flushed with nitrogen for 10 min. The synthesis was initiated by transferring the AIBN solution to the NVCL solution in the reactor using a plastic syringe. The polymerization was carried out for 24 h with the reactor submerged into a 70 °C paraffin oil bath. A nitrogen balloon was used to flush the solution prior to synthesis as well as to ensure nitrogen atmosphere throughout the synthesis. Total volumes of 1,4-dioxane ranging from 40 to 400 mL were used, while the concentration of NVCL in 1,4-dioxane was maintained at 0.16 mol/L and the NVCL/AIBN molar ratio was kept constant at 7:1.

2.2.2. Purification of PNVCL. After polymerization, 1,4-dioxane was evaporated overnight using a rotary evaporator (RV 8 pro V, IKA Works, Inc., Staufen im Breisgau, Germany) at 20 mbar and 40 rpm. After evaporation of 1,4-dioxane, the resulting PNVCL was dissolved in ultrapure water to obtain a concentration of approximately 200 mg/mL. The polymer solution was dialyzed using a Pur-A-Lyzer dialysis cassette (MWCO 3.5 kDa, Sigma-Aldrich, Søborg, Denmark) against ultrapure water, at a polymer solution-to-water ratio of 1:50. The dialysis was conducted for 72 h and the water was changed after the first 8 h. The polymer solution was aliquoted from the dialysis cassette into small glass beakers for freeze-drying. Freeze-drying was carried out using an Epsilon 2−4 LSC shelf apparatus (Martin Christ, Osterode am Harz, Germany). First, the polymer solution was cooled to −30 °C over 3 h. The temperature was maintained at −30 °C for an additional 3 h. The pressure was then reduced to 0.12 mbar over 10 min, followed by a gradual increase to 0 °C over 1 h and 20 min. The drying process was continued for 16 h and 30 min. After drying, the PNVCL powder was stored in sealed glass vials at 5 °C and ambient humidity. The yield was calculated from dry PNVCL mass and initial NVCL mass by eq 1. The mean and standard deviation (SD) were determined for n batch replicates (n_B) = 7.

$$\text{Yield}[\%] = \frac{m_{\text{polymer}}}{m_{\text{monomer}}} \times 100 \quad (1)$$

2.2.3. Assessment of Monomer-to-Polymer Conversion and Purity. Nuclear magnetic resonance (NMR) spectroscopy was conducted using a Bruker Avance III 600 MHz NMR spectrometer (Bruker Biospin, Billerica, MA, USA) equipped with a Bruker SampleJet autosampler and a 1.7 mm TCI cryoprobe, employing standard Bruker pulse sequences to acquire ^{1}H NMR and ^{13}C NMR spectra. Samples of NVCL and PNVCL were prepared at 10 mg/mL in $CDCl_3$. Visualization and data treatment of NMR spectra were performed in MestReNova 15.1.0 (Mestrelab Research S.L., Santiago de Compostela, Spain). All spectra were aligned according to $CDCl_3$ (^{1}H NMR, 7.26 ppm; ^{13}C NMR, 77.0 ppm). Monomer-to-polymer conversion was calculated from the NMR spectra obtained prior to purification (Supporting Information, Figure S1D). Integrals were computed in MestReNova 15.1.0 (Mestrelab Research S.L.) for NMR peaks assigned to vinyl protons for NVCL (7.35 ppm, H_g) and the caprolactam ring unaffected by polymerization (2.4 ppm, H_b). The integrals were normalized to the number of protons per peak (n). The conversion was calculated by eq 2.

$$\text{Conversion}[\%] = 1 - \frac{I(H_g)/n(H_g)}{I(H_b)/n(H_b)} \quad (2)$$

2.3. Determination of PNVCL Molecular Weight

2.3.1. Gel Permeation Chromatography (GPC). GPC was carried out using high-performance liquid chromatography (HPLC). Measurements were performed using a RID-20A Shimadzu differential refractive index detector, a SIL-20AC Shimadzu autosampler and an LC-20AD Shimadzu pump (Shimadzu Scientific Instruments, Columbia, MD, USA). PNVCL was dissolved in DMF at a concentration of 1 mg/mL and passed through a 20 μm polytetrafluoroethylene (PTFE) filter prior to measurements. DMF with 10 mM LiCl was used as the mobile phase and measurements were performed on an Asahipak GF-310 HQ (Showa Denko K.K., Tokyo, Japan) 7.5 × 300 mm column with a flow rate of 0.5 mL/min at 40 °C. Polyethylene glycol (PEG) monodisperse standards (Polymer Laboratories, Amherst, MA, USA) were likewise dissolved in DMF at a concentration of 1 mg/mL and passed through a 20 μm PTFE filter prior to analysis. A calibration curve was formed from the elution peaks of six standards with sizes of 282, 499, 1080, 1470, 4020, and 6450 g/mol. Number-average molecular weight (M_n) and weight-average molecular weight (M_w) of PNVCL were determined from the calibration curve. GPC chromatograms for four PNVCL batches are included in Supporting Information (Figure S10). The mean and SD were determined for n_B = 4.

2.3.2. Osmometry. Osmometric measurements were conducted using an osmometer (Type 7M, Löser, Berlin-Spandau, Germany) measuring osmolality [mOsm/kg]. PNVCL samples were prepared at three different concentrations; 10, 20, and 30 mg/mL in ultrapure water. Technical replicates (n_t) = 3 were performed for each concentration. All osmolarity measurements were recalculated into M_n before determining the mean and SD for n_B = 6.

2.3.3. Matrix-Assisted Laser/Desorption Ionization Mass Spectrometry (MALDI-MS). MALDI-MS was performed using a Bruker SolariX XR 7T ESI/MALDI-FT-ICR mass spectrometer (Bruker, Bremen, Germany). PNVCL was dissolved in DCM followed by dissolution in a 5 mg/mL solution of super-DHB in DCM. A 1 μL sample of this solution was transferred to a ground steel target. The detection range was m/z 150 to 4000. External calibration was performed using NaTFA cluster ions. The mass spectra were analyzed using Bruker DataAnalysis 5.0 software (Bruker) and average values of M_n and M_w were calculated from each spectrum. A range is reported for n_B = 2.

2.3.4. Diffusion-Ordered Spectroscopy (DOSY)-NMR. DOSY-NMR spectroscopy was performed using a Bruker Avance III 500 MHz with a 1.7 mm TCI cryoprobe using standard Bruker pulse sequences. Samples of PNVCL were prepared at a concentration of 20 mg/mL in D_2O. Visualization and data treatment of DOSY-NMR spectra were performed in MestReNova 15.1.0 (Mestrelab Research S.L., Santiago de Compostela, Spain). The hydrodynamic radius (R_h) is available from the diffusion coefficient measured by DOSY-NMR, which is related to the molecular weight via the equation $R_h = k[M]^{\alpha}$. Since the actual values for the constants k and α are unknown in this case, the default software settings were used for calculating M_w. The mean and SD were determined for n_B = 3.

2.4. Solid State Characterization of PNVCL

X-ray powder diffraction (XRPD) was performed using an X-ray powder diffractometer (X'Pert PRO, Malvern PANalytical, Westborough, MA, USA). A PNVCL powder sample (4 mg) was loaded onto an aluminum sample holder and the analysis was performed over a 2θ range of 5° to 35° at a scan speed of 0.020°/s.

Thermogravimetric analysis (TGA) was conducted using a thermogravimetric analyzer (Discovery, TA Instruments Inc., New Castle, DE, USA). A PNVCL powder sample (8 mg) was loaded on an open platinum pan and heated from 20 to 400 °C at a rate of 10 °C/min. Data were analyzed using TRIOS software (version 5.1), and weight loss in the 20 to 100 °C temperature range was quantified. The mean and SD were determined for n_B = 3.

2.5. Characterizing Thermoresponsive Properties of PNVCL

2.5.1. Thermo-Moisture Chamber. The thermo-moisture-responsive behavior of PNVCL was studied by incubating PNVCL powder at varying temperatures (20 and 50 °C) and humidity conditions (ambient humidity and 100% humidity) for 4 h. PNVCL powder samples (4 mg) were deposited on a carbon mat in an

https://doi.org/10.1021/acsapm.6c02142
ACS Appl. Polym. Mater. XXXX, XXX, XXX−XXX

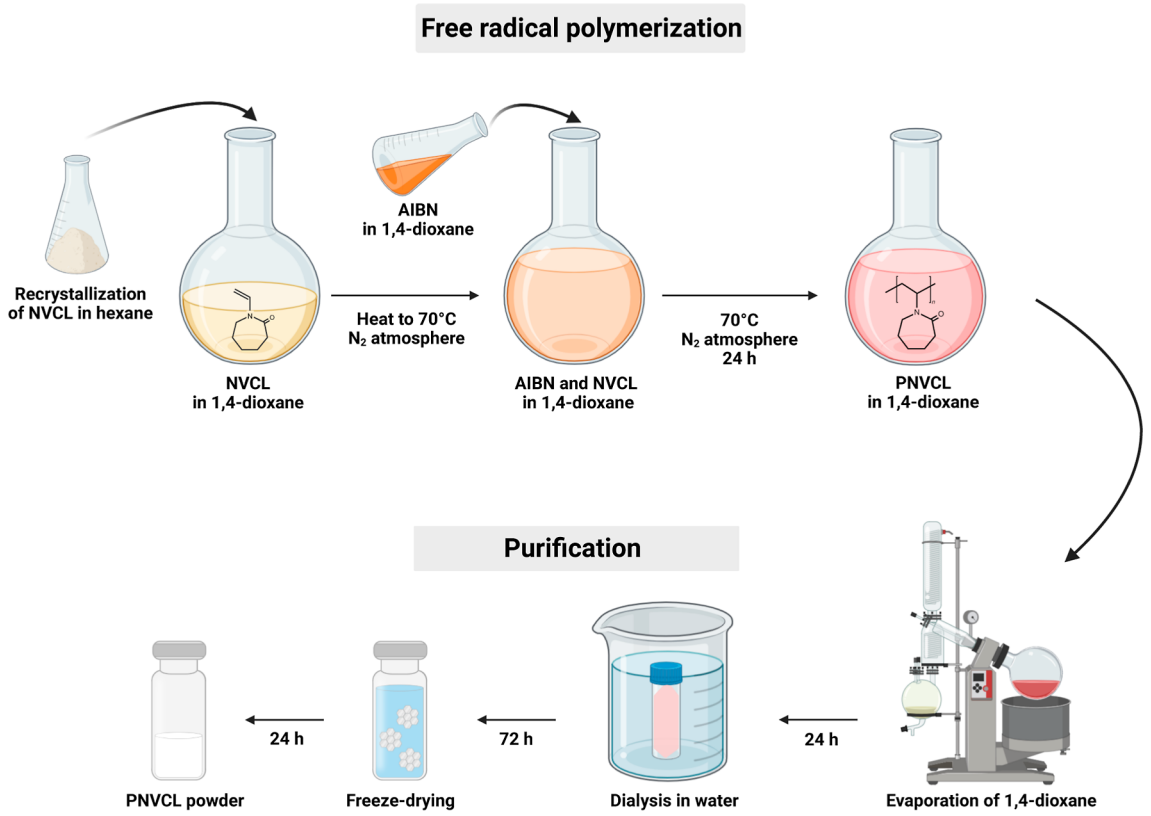

Figure 1. Illustration of the optimized process of PNVCL synthesis by free radical polymerization and purification by solvent evaporation, dialysis and freeze-drying. Created in BioRender. Gregersen, C.H. (2026) https://BioRender.com/u2ycj5i.

aluminum capsule, which was then placed inside a Petri dish with a lid, either filled with 10 mL ultrapure water (100% humidity) or left empty (ambient humidity). The Petri dish was placed in an incubator at 20 or 50 °C. Scanning electron microscopy (SEM) (TM3030, Hitachi, Tokyo, Japan) was used to visualize the morphology of the polymer directly on the carbon mat, before and after being subjected to temperature and/or humidity. Prior to SEM imaging, samples were sputter-coated with gold (Cressington 108 auto, Ted Pella Inc., Redding, CA, USA) for 30 s under argon atmosphere.

2.5.2. LCST. To evaluate the LCST, the absorbance of PNVCL dissolved in ultrapure water was recorded at 570 nm using a ultraviolet−visible (UV−vis) spectrophotometer (CLARIOstar plate reader, BMG Labtech, Ortenberg, Germany) during temperature ramping from 24 to 50 °C in increments of 2 °C every 10 min. PNVCL was dissolved in ultrapure water at concentrations of 10, 20, 50, and 100 mg/mL by stirring for 24 h under ambient conditions. All samples were transferred to a 96-well plate (Nunc, black/clear bottom, Thermo Fisher Scientific, Waltham, MA, USA) in triplicates (n_t = 3), and the plate was sealed with adhesive sealing tape (Nunc, Thermo Fisher Scientific) to prevent solvent evaporation. Absorbance measurements were converted to transmittance and the LCST was determined as the temperature where the transmittance approached 0%.[23] The mean and SD were determined for n_B = 3 using this approach. In addition, the derivatives of the transmittance−temperature curves are included in Supporting Information (Figure S11).

2.5.3. Raman Spectroscopy. Raman spectra were acquired using a THz-Raman system (Ondax Inc., Monrovia, CA, USA) equipped with a 300 mW, 785 nm diode laser as the excitation source. Backscattered Raman signals (180° geometry) were collected through a free-space optics module and passed through a set of volume Bragg gratings (Ondax Inc.). The filtered signal was transmitted via fiber-optic coupling to a spectrograph (Ondax Inc.), and the dispersed light was detected using a CCD detector (Andor iVac 316, Oxford Instruments, Belfast, UK). Spectra were recorded across a range of −870 to 3200 cm^{-1}, with a spectral resolution between 4 and 6 cm^{-1}. For temperature-dependent measurements, approximately 10 mg of PNVCL powder or 50 μL hydrated PNVCL (1000 mg/mL) was placed in an aluminum sample pan (TA Instruments, New Castle, DE, USA) covered by a borosilicate glass cover and mounted on a PE120 variable-temperature stage controlled by a T95 system controller (Linkam Scientific Instruments Ltd., Tadworth, UK). The sample was first equilibrated at 20 °C for 5 min, then heated to 50 °C at a rate of 1 °C/min, held at that temperature for an additional 5 min, and subsequently cooled (this additional step was used for the analysis of hydrated PNVCL) to 20 °C at the same rate. Temperature tracking during the spectral acquisition was established through manual correlation across multiple sample runs. Each spectrum consisted of 10 coadded scans, with an integration time of 0.5 s per scan, allowing for a temperature resolution of approximately 0.08 °C during variable-temperature experiments. Data collected during the heating and cooling were analyzed independently, following a similar procedure as previously described.[24] Initial preprocessing was carried out using Spectragryph 1.2.16.1 software (Menges Instruments, Oberstdorf, Germany) to remove cosmic ray artifacts (≤3 pixels wide). Varied baseline corrections were applied separately to each spectral region using the spectroscopy module in Orange Data Mining 3.37.0 (University of Ljubljana, Ljubljana, Slovenia). In the low-frequency Raman (LFR) region (−300 to 300 cm^{-1}), a linear baseline correction was applied, while in the midfrequency Raman (MFR) region (500−1725 cm^{-1}), a rubberband baseline correction was applied due to the curved nature. Standard normal variate (SNV) transformation was used to adjust for scale and scattering variations in the MFR region (500−1725 cm^{-1}) and part of the LFR region (10−200 cm^{-1}). Principal component analysis (PCA) was subsequently performed on preprocessed Raman spectra using the PCA widget with default settings in the Orange Data Mining 3.37.0 (University of Ljubljana) software.

2.5.4. Small-Angle X-ray Scattering (SAXS) and Wide-angle X-ray Scattering (WAXS). SAXS and WAXS measurements were performed using a Nano-InXider (Xenocs, Grenoble, France)

https://doi.org/10.1021/acsapm.6c02142
ACS Appl. Polym. Mater. XXXX, XXX, XXX−XXX

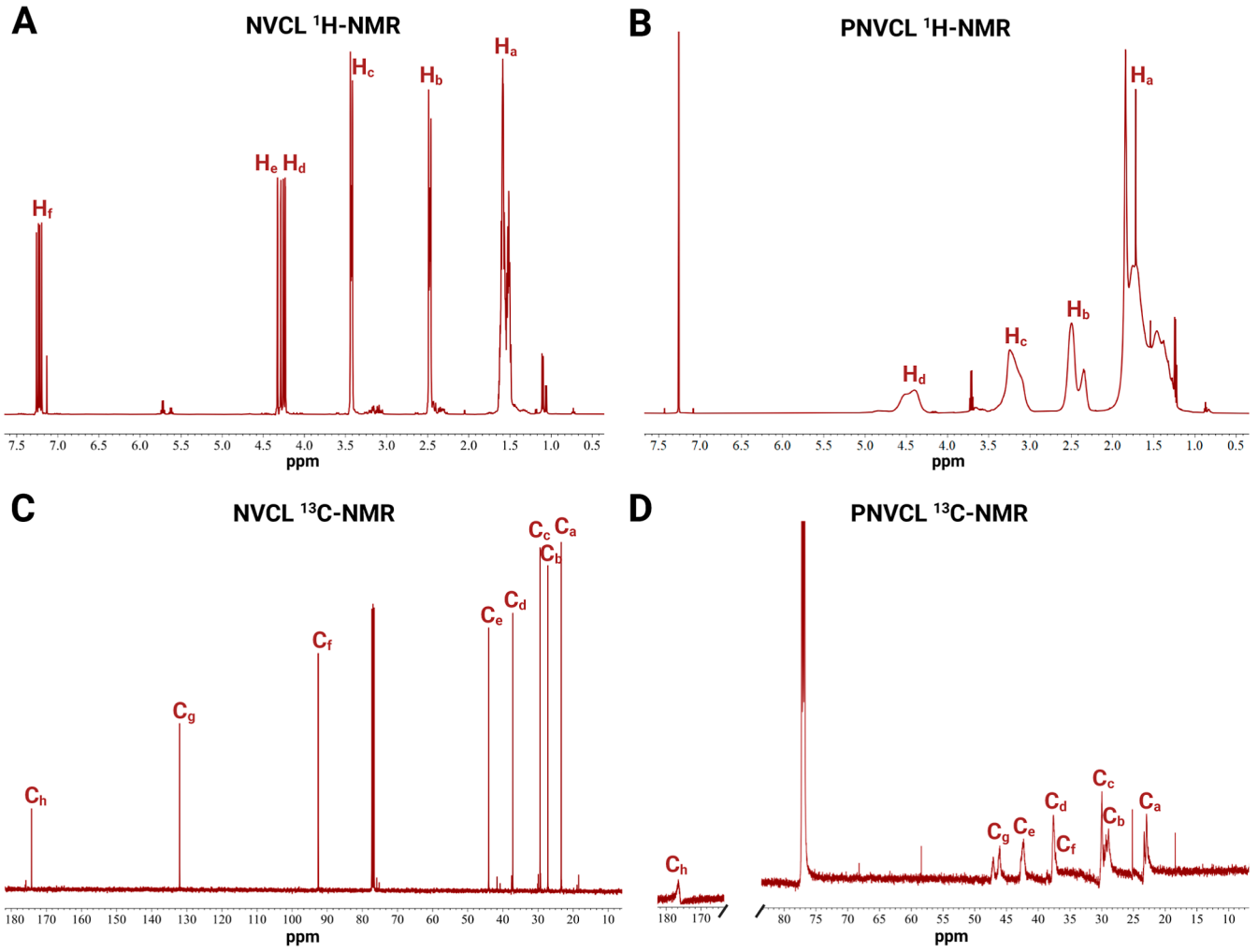

Figure 2. ^{1}H NMR spectra of (A) NVCL and (B) PNVCL and ^{13}C NMR spectra of (C) NVCL and (D) PNVCL. Hydrogen and carbon groups (denoted H_x and C_x, respectively) are specified in Table 1. The NMR spectra for PNVCL are representative of all synthesized PNVCL batches (n_B = 7).

equipped with a Cu Kα source with a 1.54 Å wavelength and a two-detector setup enabling simultaneous SAXS/WAXS acquisition. Measurements were conducted using a medium-resolution setup with a beam size of 800 μm and a total q-range of 0.011 to 4.25 Å^{-1}. Hydrated PNVCL (1000 mg/mL) or dissolved PNVCL (100 mg/mL) were loaded into glass capillaries (Mark-tubes, Hilgenberg, Germany). Two temperature series were recorded during heating (20 to 50 °C) followed by cooling (50 to 20 °C); one in 2 °C increments with a dwell time of 5 min per step, and one in 1 °C increments with a dwell time of 15 min per step. As both these data sets showed high similarity, only the latter data set is reported. Data were masked, radially averaged, and corrected for background scattering from sample cell and water in the XSACT software (Xenocs). SAXS data in the q-range of 0.02 to 0.2 Å^{-1} were fitted using a unified fit model[25] to extract the radius of gyration (R_g) from each scattering profile. Fitting was performed in SasView (SasView Project, San Francisco, CA, USA) using the batch fitting option with the chain-fit feature enabled, such that fit parameters from each temperature step were used as initial parameters for the subsequent fit.

2.6. Data Visualization and Statistical Analysis

The data visualization was performed in GraphPad Prism 10.0, unless otherwise stated. All data presented as mean ± SD were collected as batch replicates and/or technical replicates, which is specified for the individual data. Statistical analysis was conducted on the LCST data using one-way ANOVA followed by Tukey's multiple comparisons test, with individual group means compared pairwise.

3. RESULTS AND DISCUSSION

3.1. PNVCL Synthesis from NVCL by Free Radical Polymerization

Standardized and reproducible protocols for PNVCL synthesis are highly needed, as persistent challenges in achieving controlled polymerization of NVCL have hindered broader application of PNVCL.[6,7] The synthesis and purification workflow (Figure 1) was designed and optimized to ensure complete monomer conversion and efficient removal of 1,4-dioxane prior to further characterization. The duration of synthesis differed significantly between otherwise comparable reports,[9,26] which created a direct incentive for our investigations. A short duration of synthesis of 3 and 4 h did not result in complete monomer-to-polymer conversion, leading us to evaluate an extended duration of synthesis of 24 h. Complete monomer-to-polymer conversion after 24 h was confirmed by an ^{1}H NMR signal corresponding exclusively to PNVCL. The 1,4-dioxane evaporation process was subsequently optimized and evaluated using ^{1}H NMR analysis of samples collected after 24 and 48 h rotary evaporation. This led us to move forward with a duration of 24 h, since 48 h did not remove substantially more 1,4-dioxane, and other purification methods were therefore explored. The duration

https://doi.org/10.1021/acsapm.6c02142
ACS Appl. Polym. Mater. XXXX, XXX, XXX−XXX

Table 1. Identified Peak Ranges from ^{1}H NMR and ^{13}C NMR Spectra Corresponding to Specific Hydrogen and Carbon Environments (Denoted H_x and C_x, Respectively) within the Molecules of NVCL and PNVCL

NVCL	^{1}H-NMR shift [ppm]
H_a	1.6
H_b	2.4
H_c	3.4
H_d	4.2
H_e	4.3
H_f	7.1

PNVCL	^{1}H-NMR shift [ppm]
H_a	1.7
H_b	2.4
H_c	3.1
H_d	4.4

NVCL	^{13}C-NMR shift [ppm]
C_a	23
C_b	27
C_c	29
C_d	37
C_e	44
C_f	9
C_g	132
C_h	174

PNVCL	^{13}C-NMR shift [ppm]
C_a	23
C_b	29
C_c	30
C_d	38
C_e	42
C_f	37
C_g	46
C_h	176

of dialysis was also optimized and evaluated using ^{1}H NMR analysis of samples collected after 0, 24, 48, and 72 h dialysis. On this basis, dialysis for 72 h was selected to remove as much 1,4-dioxane as possible. The results from the optimization studies are provided in the Supporting Information (Figures S1−S3).

3.1.1. Structural Conformation of PNVCL Confirmed by NMR Spectroscopy. NMR spectroscopy was used to quantify the conversion of NVCL to PNVCL and to assess the purification process. Both ^{1}H NMR and ^{13}C NMR spectra from NVCL and PNVCL were acquired (Figure 2), while the identified peaks corresponding to specific proton and carbon groups within the molecules were identified (Table 1).

In the ^{1}H NMR spectra, PNVCL (Figure 2B) expectedly exhibited broader peak widths than NVCL (Figure 2A), reflecting reduced spectral resolution due to polymer formation. Notably, the peaks associated with the vinyl protons of NVCL (H_e, H_f) were absent in the PNVCL spectrum, confirming complete polymerization within the resolution of NMR. Correspondingly, the ^{13}C NMR spectrum of PNVCL (Figure 2D) displayed shifts in several peak positions compared to NVCL (Figure 2C), with the most pronounced changes observed for the vinyl-associated carbons. These carbons shifted substantially upon polymerization, consistent with the opening of the carbon−carbon double bonds to facilitate the formation of a polyvinyl backbone. In contrast, peaks associated with the caprolactam ring remained largely unchanged, indicating preservations of the caprolactam ring structure during polymerization. These spectral features are consistent with those of commercially available PNVCL from Polymer Source Inc. with M_v = 1800 g/mol (Supporting Information, Figure S4) and are in general agreement with literature reports.[17,26] The conversion from NVCL to PNVCL was calculated as 97% prior to purification. The purification of PNVCL was further evaluated by NMR spectroscopy, with particular attention to residual solvent peaks and impurities. Solvent peaks arising from $CDCl_3$ were observed at 7.26 ppm in the ^{1}H NMR spectrum and 77.0 ppm in the ^{13}C NMR spectrum. In addition, a minor peak at 3.71 ppm in the ^{1}H NMR spectrum and 67.14 ppm in the ^{13}C NMR spectrum suggested the presence of a trace amount of 1,4-dioxane still remaining after purification, in correspondence with earlier reports from both 1,4-dioxane and other solvents.[10,17] The peak at 1.56 ppm in the ^{1}H NMR spectrum of PNVCL (Figure 2B) was attributed to residual water, which is likely present due to the hygroscopic nature of PNVCL retaining water even after freeze-drying. This was supported by TGA thermograms (Supporting Information, Figure S5A), revealing an initial weight loss of 4.0 ± 1.0% (n_B = 3) in the temperature range of 20−100 °C, which can be attributed to evaporation of residual water in the PNVCL powder. The yield was calculated to be 33 ± 12% (n_B = 7).

3.2. Molecular Weight Characteristics of Synthesized PNVCL

The molecular weight of PNVCL is a critical parameter to assess and control, due to it being a key influencing factor on the thermoresponsive behavior of the polymer. The relationship between LCST and molecular weight is well established, with increasing molecular weight yielding a lower LCST.[9,19] However, challenges in accurately determining the molecular weight of PNVCL have been reported in literature, largely due to difficulties in obtaining reliable results from using conventional methods such as GPC.[10,26,27] Thus, in this study, the molecular weight of the synthesized PNVCL was determined using four complementary techniques, namely GPC, osmometry, MALDI-MS, and DOSY-NMR. This multimethod approach enabled the generation of reliable molecular weight estimate while also providing a methodological reference for future PNVCL characterization (Table 2). We focused on a single molecular weight PNVCL, to enable comparability between methods.

The synthesized PNVCL exhibited low molecular weight (Table 2), yet comparable to previously reported values.[28,29] It is well established that the molecular weight of PNVCL can

https://doi.org/10.1021/acsapm.6c02142
ACS Appl. Polym. Mater. XXXX, XXX, XXX−XXX

Table 2. Molecular Weight of PNVCL Determined Using GPC (M_n and M_w), Osmometry (M_n), MALDI-MS (M_n and M_w), and DOSY-NMR (M_w), as Well as Dispersity (M_w/M_n) Determined Using GPC and MALDI-MS[a]

	GPC	Osmometry	MALDI-MS	DOSY-NMR
M_n	715 ± 81	1513 ± 756	1823;1994	
M_w	1215 ± 219		2324;2404	4880 ± 789
M_w/M_n	1.7 ± 0.1		1.2;1.3	

[a]The results for M_n and M_w are reported in g/mol for PNVCL synthesized with the optimized protocol as mean ± SD of n_B = 4 for GPC, n_B = 6 for osmometry, and n_B = 3 for DOSY-NMR. The results from MALDI-MS are reported as a range for n_B = 2.

vary significantly, with reported values from 1140 g/mol to 2,340,000 g/mol, depending on the synthesis method and the choice of solvent, initiator, and chain transfer agent.[12,29] The different analytical techniques employed in this study yielded slightly varying molecular weight estimates, attributed to the distinct principles and the inherent assumptions introduced with each technique. In correspondence to previous reports,[26,27] GPC analysis initially proved challenging due to overlap between the tetrahydrofuran (THF) solvent peak and the PNVCL peak. This issue was resolved by changing the solvent to DMF, which provided clear separation between the solvent and PNVCL peaks. GPC estimates molecular weight based on hydrodynamic volume, however calibrating with a standard of comparable chain geometry and behavior in the chosen solvent can minimize the impact of hydrodynamic and geometric assumptions on the derived molecular weight. Osmometry was used to determine the osmolality of a known concentration of PNVCL in water [Osm/kg] which was subsequently recalculated to M_n. A known limitation of colligative property-based techniques such as osmometry is underestimation of high molecular weight fractions relative to low molecular weight fractions.[30] MALDI-MS provided the mass distribution of individual polymer chains from which both M_n and M_w were determined. The preferential ionization of low molecular weight fractions causes the sensitivity of this method to decline with increasing molecular weight, making it ideal for our low molecular weight polymer.[31] DOSY-NMR determines molecular diffusion coefficients, which are converted to R_h and subsequently to M_w. This conversion assumes spherical molecular geometry, which is a much simplifying assumption for PNVCL that could contribute to the overestimation of molecular weight relative to the other three techniques. Across all applied methods (Table 2), the synthesized PNVCL consisted of approximately 5−35 repeat units per polymer chain. GPC and MALDI-MS were further used to measure the dispersity, which was in the range of 1.2−1.8, and thereby slightly lower than that previously reported for PNVCL synthesized by free radical polymerization, generally associated with high dispersity.[6,7,9] More controlled polymerization techniques, such as atom transfer radical polymerization (ATRP) or reversible addition−fragmentation chain transfer (RAFT) polymerization, may provide polymers with lower dispersity, but come with a cost of more complex polymerization procedures.[6,32]

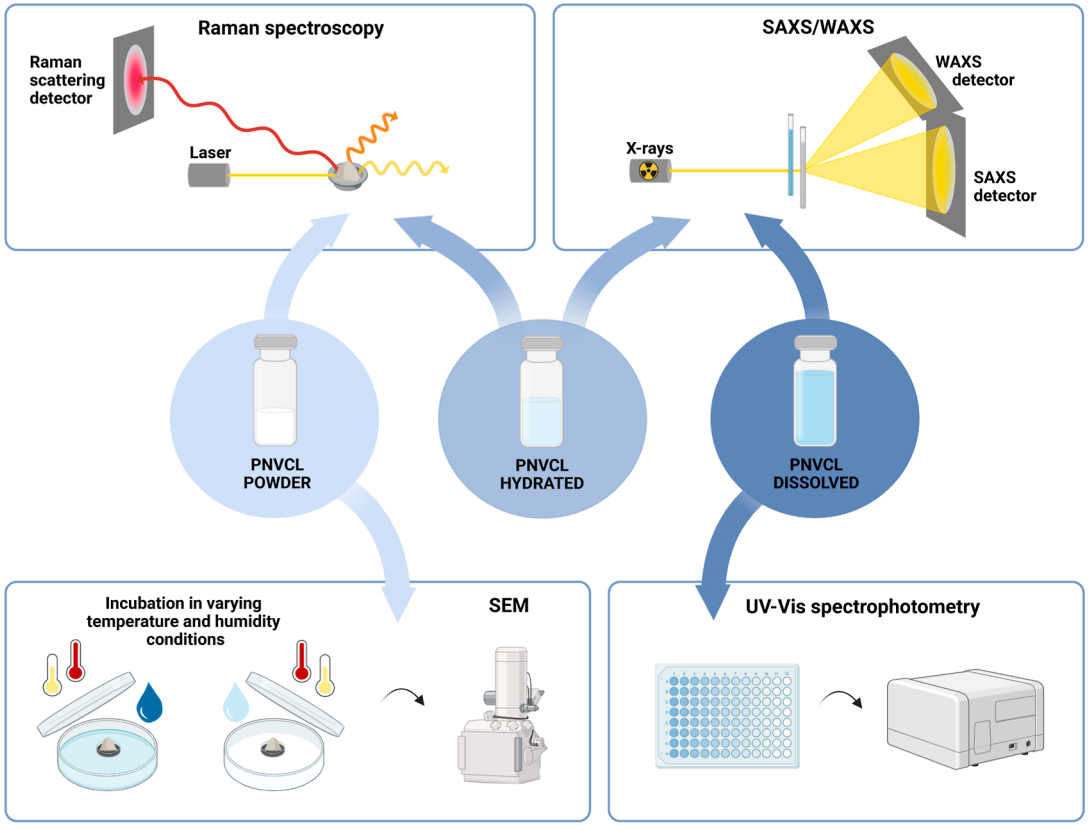

Figure 3. Illustration of methods applied to evaluate the thermoresponsive properties of PNVCL in powder form, in hydrated state (1000 mg/mL) and in solution (10−100 mg/mL). Methods include SEM, UV−vis spectrophotometry, Raman spectroscopy and SAXS/WAXS. Created in BioRender. Gregersen, C.H. (2026) https://BioRender.com/6uc3ttj.

https://doi.org/10.1021/acsapm.6c02142
ACS Appl. Polym. Mater. XXXX, XXX, XXX−XXX

3.3. Characterization of the Thermoresponsive Properties of PNVCL

The thermoresponsive properties of PNVCL were assessed across various hydration states using complementary characterization techniques, including SEM, UV−vis spectrophotometry, Raman spectroscopy, and SAXS/WAXS (Figure 3).

3.3.1. PNVCL Powder Displays Film-Forming Properties at High Humidity Independent of Temperature. The morphological response of PNVCL powder to temperature and humidity was studied by incubating PNVCL under various thermo-moisture conditions, followed by SEM imaging. Temperatures below the LCST (20 °C) and above the LCST (50 °C) were examined in combination with varying humidity conditions (Figure 4).

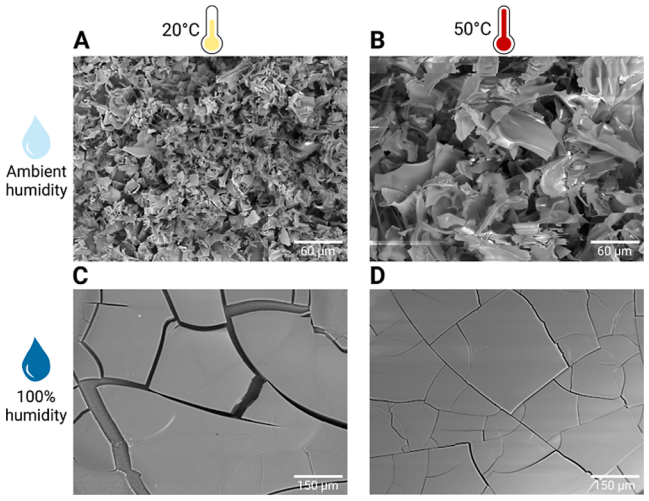

Figure 4. Thermo-moisture-responsive behavior of PNVCL powder, studied by incubation at different temperatures (20 or 50 °C) and humidity levels (ambient humidity or 100% humidity) for 4 h followed by SEM imaging. (A) 20 °C, ambient humidity; (B) 50 °C, ambient humidity; (C) 20 °C, 100% humidity; (D) 50 °C, 100% humidity. The SEM images are representative of at least $n_B = 3$.

SEM images of PNVCL powder incubated under ambient humidity (Figure 4A,B) indicated structure preservation upon increasing the temperature from 20 to 50 °C, although the polymer structures appeared larger. SEM images of PNVCL subjected to 100% humidity (Figure 4C,D) revealed film formation at both 20 and 50 °C. A variation in film morphology was observed, and the higher temperatures seemed to result in reduced size of the cracks in the film. According to TGA thermograms (Supporting Information, Figure S5A), the PNVCL powder contains 4.0 ± 1.0% ($n_B = 3$) water. It was evident that the residual water was not sufficient to act as a plasticizer and cause film formation, in comparison to that observed with 100% humidity at 20 °C (Figure 4C). The film-forming properties of PNVCL are exploited in the commercially available product Luviskol® Plus by BASF, which is marketed as a film-forming agent for hair care products.[4] Only a few other studies report on PNVCL films. For example, Zhao et al.[33] combined PNVCL and poly(2-hydroxypropyl acrylate) (PHPA) in a thermoresponsive layer-by-layer film and studied the dissolution process as a function of temperature. Similarly, Kharlampieva et al.[34] constructed layer-by-layer films from PNVCL and poly(methacrylic acid) (PMAA), which exhibited temperature-dependent dye permeability of the film. Lee et al.[35] created PNVCL films that changed from hydrophilic to hydrophobic when increasing the temperature above the LCST, and that was exploited for temperature-controlled attachment and detachment of cultured cells. However, the film-forming properties of PNVCL have yet to be explored further for its potential in drug delivery applications.

3.3.2. PNVCL in Solution Exhibits Concentration-Dependent LCST. As the LCST has been reported to cohere with polymer concentrations,[6] four different PNVCL concentrations were evaluated for their LCST (Figure 5).

UV−vis spectrophotometry is the most commonly used method for determining the LCST of PNVCL, as it enables detection of an abrupt decrease in transmittance associated with PNVCL precipitation from solution.[7] This sudden decrease in transmittance arises from the coil-to-globule conformational transition occurring around the LCST, during which PNVCL changes from a hydrophilic to a hydrophobic state. In the present study, PNVCL exhibited significantly different LCST values in the range of 38 to 48 °C, when lowering the concentration from 100 to 10 mg/mL (Figure 5). These findings are consistent with previously reported LCST values between 32 and 50 °C for PNVCL concentrations ranging from 0.5 to 15% (w/v) (corresponding to 5 to 150 mg/mL), supporting our findings.[6] The low SD of maximum 1 °C found across three individually synthesized PNVCL batches is an important finding to ensure consistent LCST values

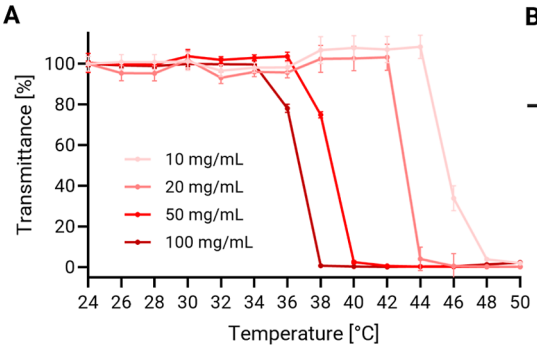

B

PNVCL concentration in water [% (w/v)]	LCST
10 mg/mL	47 ± 1 °C
20 mg/mL	43 ± 1 °C
50 mg/mL	40 ± 0 °C
100 mg/mL	39 ± 1 °C

***
***
*
***

Figure 5. Concentration dependence of LCST. (A) Transmittance at 570 nm (reported as % of transmittance at ambient conditions) for PNVCL dissolved in water at varying concentrations (10, 20, 50, 100 mg/mL) during heating from 24 to 50 °C. Data are reported as mean ± SD ($n_t = 3$). (B) LCST reported as mean ± SD ($n_B = 3$). Statistical comparisons were conducted using one-way ANOVA followed by Tukey's multiple comparisons test, where $*p < 0.05$, $**p < 0.01$, $***p < 0.001$.

https://doi.org/10.1021/acsapm.6c02142
ACS Appl. Polym. Mater. XXXX, XXX, XXX−XXX

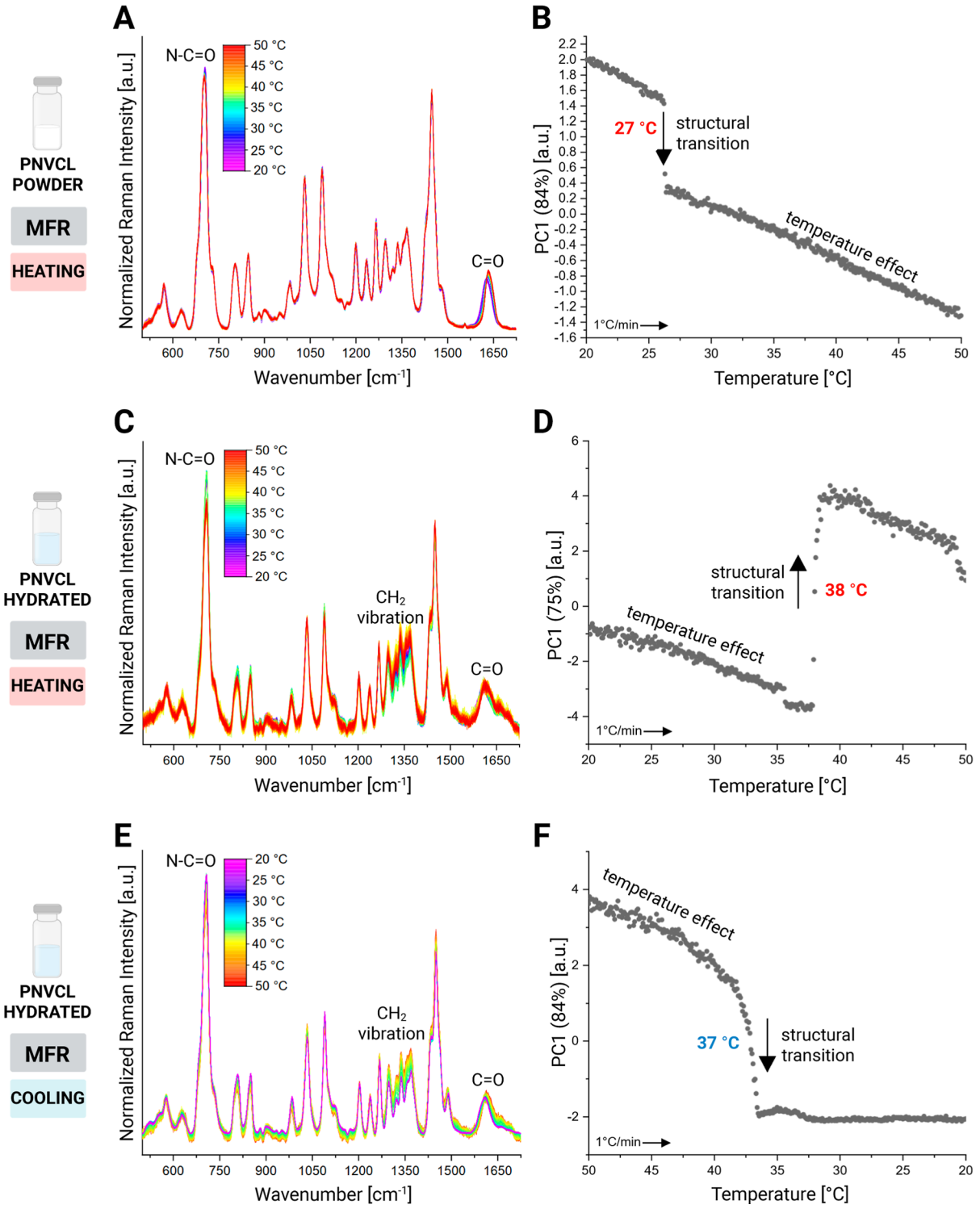

Figure 6. MFR spectra for PNVCL powder during heating from 20 to 50 °C and hydrated PNVCL (1000 mg/mL) during heating from 20 to 50 °C and cooling from 50 to 20 °C (n_B = 1). (A) MFR variable temperature spectra of PNVCL powder, (B) PC1 scores plot corresponding to the MFR spectra of PNVCL powder. (C) MFR variable temperature spectra of hydrated PNVCL during heating, (D) PC1 scores plot corresponding to the MFR spectra of hydrated PNVCL during heating, (E) MFR variable temperature spectra of hydrated PNVCL during cooling, (F) PC1 scores plot corresponding to the MFR spectra for hydrated PNVCL during cooling.

across batches (Figure 5B). The broad LCST range associated with varying PNVCL concentrations must be carefully considered when designing a thermoresponsive PNVCL-based drug delivery system. In particular, dilution upon administration by e.g. injection may shift the LCST from body temperature to higher temperatures, thereby compromising the desired temperature-triggered responsiveness of the drug delivery system. Based on the present results, PNVCL concentrations should be above approximately 100 mg/mL in water to enable PNVCL collapse at body temperature, a prerequisite for stimuli-responsive behavior. Although this threshold will vary with the molecular weight of the polymer

https://doi.org/10.1021/acsapm.6c02142
ACS Appl. Polym. Mater. XXXX, XXX, XXX−XXX

and the employed solvent composition, it is clear that changes in polymer concentration following administration must always be accounted for when considering the administration route and potential dilution of a PNVCL-based drug delivery system. Accordingly, formulation strategies should account for the anticipated degree of dilution or evaporation after administration, for example through adjustment of the initial polymer concentration to compensate for these changes, thereby maintaining the desired thermoresponsive behavior for the intended route of administration, dosage form, and specific indication.

3.3.3. Raman Spectroscopy Elucidates Chemical Shifts Around the LCST. Raman spectroscopy was employed to investigate temperature-dependent structural changes of PNVCL across multiple length scales. MFR spectroscopy primarily probes intramolecular vibrations and local chemical environments, enabling monitoring of changes in chemical bonding and chain conformation during heating and cooling. In contrast, LFR spectroscopy is sensitive to collective, long-range motions and intermolecular interactions, including polymer−polymer interactions and chain packing associated with aggregation. By interrogating these distinct but complementary vibrational regimes, MFR and LFR together may provide insight into the changes in polymer structure at the onset of aggregation around the LCST, albeit through different spectral signatures and characteristic length scales. Their combined application is therefore expected to yield complementary, multiscale information on the molecular mechanisms underlying the LCST-driven coil-to-globule transition of PNVCL. To the best of our knowledge, this study represents the first temperature-dependent Raman spectroscopy investigation of PNVCL. PNVCL was initially studied in powder form to assess its thermoresponsive behavior in the lowest achievable hydration state, containing approximately 4% bound water (Supporting Information, Figure S5A). In addition, a hydrated PNVCL sample (1000 mg/mL) was included to mimic the expected hydrated state following cutaneous application of e.g. a film-forming system. Both powder and hydrated PNVCL samples were analyzed during heating from 20 to 50 °C, while subsequent cooling from 50 to 20 °C was carried out for the hydrated sample. MFR spectra (Figure 6) and LFR spectra (Supporting Information, Figure S6) were obtained. PCA was performed on all data sets to reduce spectral dimensionality and facilitate comparison of temperature-dependent changes. Across all conditions, the first principal component (PC1) accounted for 75−98% of the total spectral variance (Figure 6, right side panel). Corresponding PC1 loadings plots are also provided (Supporting Information, Figure S7).

Raman data (Figure 6) first revealed a general temperature-dependent effect in both MFR and LFR spectra, primarily arising from typical thermal responses of vibrational modes such as gradual peak redshifting and line width changes. This effect manifested in the PC score plots as largely linear trends with increasing or decreasing temperature. Superimposed on this continuous temperature-driven behavior, distinct thermoresponsive structural changes of PNVCL were observed, with clear transitions captured by PC1. These transitions were evident in both MFR and LFR data and differed between hydration states.

For PNVCL powder, MFR spectra (Figure 6A) displayed temperature-dependent spectral changes dominated by shifts in peak position rather than changes in absolute intensity. In particular, a pronounced shift of the carbonyl-associated band at ∼1635 cm^{-1} was observed upon heating, accompanied by more subtle spectral changes in the lower wavenumber region at ∼700 cm^{-1}. The corresponding PC1 scores plot (Figure 6B) showed that these spectral changes occurred abruptly at around 27 °C, indicating a distinct structural transition. The spectral features responsible for this separation are identified in the corresponding PC1 loadings plot (Supporting Information, Figure S7B). The loadings show opposing contributions from the carbonyl-associated band around ∼1635 cm^{-1}, assigned to the caprolactam ring,[36] and features in the region around ∼700 cm^{-1} related to N−C═O vibrations.[37] This indicates that the transition is driven primarily by a redistribution of these spectral components. Given that the spectra are normalized, this behavior is consistent with temperature-induced peak shifts rather than changes in absolute Raman intensity. Below the LCST, PNVCL adopts an extended and hydrated chain conformation in which the C═O groups are strongly hydrogen-bonded to surrounding water molecules.[38,39] Such hydrogen bonding stabilizes the C═O bond, resulting in a lower vibrational frequency and, consequently, a Raman band appearing at slightly lower wavenumbers. Upon heating above the LCST, PNVCL undergoes a coil-to-globule transition into a more compact and hydrophobic conformation, leading to reduced hydrogen bonding between the C═O groups and water.[38,39] This loss of stabilization increases the vibrational frequency of the C═O bond, shifting the corresponding Raman band toward higher wavenumbers, consistent with the observed temperature-dependent spectral redistribution. This transition may involve reorientation of the caprolactam ring relative to the polymer backbone and increased local rigidity, both of which would be expected to increase the vibrational frequency of the C═O bond. From an LFR perspective, the PC1 scores plot (Supporting Information, Figure S6B) showed a clear deviation at approximately 27 °C, similar to that observed for MFR. This demonstrates that both intramolecular vibrational signatures and collective, low-frequency dynamics respond to the same underlying thermoresponsive event. This finding is particularly noteworthy given that the synthesized PNVCL powder contained only a minimal amount of residual water (∼4%). The observation that such a low hydration level is sufficient to induce a detectable structural reorganization highlights the strong sensitivity of PNVCL to its hydration state. It suggests that even limited water content can mediate temperature-driven rearrangements of both local and collective polymer structure, emphasizing that the thermoresponsive behavior of PNVCL is not restricted to the dissolved form of PNVCL predominantly described in existing studies.[8,10,17,19]

For hydrated PNVCL, the normalized MFR spectra recorded during heating (Figure 6C) exhibited similar temperature-dependent spectral changes primarily manifested as shifts and redistribution of spectral features rather than absolute intensity changes. However, more notable peak ratio changes were observed at ∼1350 cm^{-1}, while spectral changes in the regions around ∼700 cm^{-1} and the carbonyl-associated band around ∼1635 cm^{-1} were also retained. The corresponding PC1 scores plot (Figure 6D) revealed a pronounced structural transition at approximately 38 °C. The spectral origin of this separation is clarified by the PC1 loadings plot (Supporting Information, Figure S7D), which shows that features around ∼700 cm^{-1} contribute predominantly to the negative PC1 space, whereas bands in the ∼1350 cm^{-1} region contribute to the positive PC1 space. In addition, the carbonyl-

https://doi.org/10.1021/acsapm.6c02142
ACS Appl. Polym. Mater. XXXX, XXX, XXX−XXX

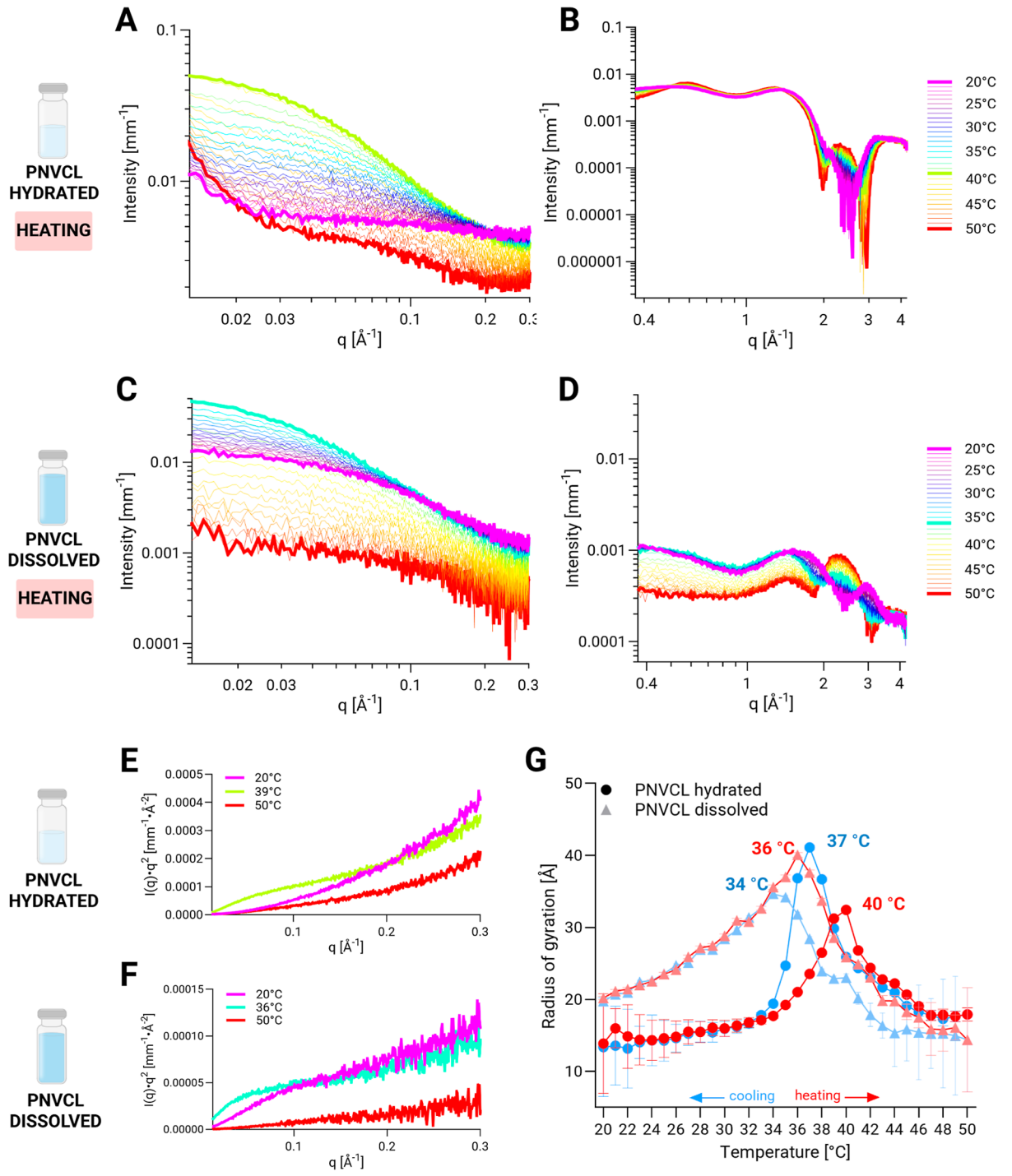

Figure 7. SAXS and WAXS data for PNVCL during heating from 20 to 50 °C (n_B = 1). (A) SAXS data and (B) WAXS data for hydrated PNVCL (1000 mg/mL) in log−log plots. (C) SAXS data and (D) WAXS data for dissolved PNVCL (100 mg/mL) in log−log plots. (E) Kratky plot for hydrated PNVCL (1000 mg/mL) at relevant temperatures. (F) Kratky plot for dissolved PNVCL (100 mg/mL) at relevant temperatures. (G) Radius of gyration (R_g) extracted from a unified fit model[25] fitted to SAXS data in the q-range of 0.02 to 0.2 Å^{-1} for both heating and cooling of dissolved and hydrated PNVCL, respectively.

associated band around ∼1635 cm^{-1} exhibits a characteristic positive−negative loading pattern, consistent with a temperature-induced peak shift rather than a change in absolute intensity. During cooling, the normalized MFR spectra (Figure 6E) followed the same temperature-dependent pathway as observed during heating. However, the PC1 scores plot (Figure 6F) showed a broader transition occurring at a slightly lower temperature of approximately 37 °C, consistent with modest hysteresis in the structural response of hydrated PNVCL. The PC1 loadings obtained during cooling (Supporting Information, Figure S7F) were similar to those from heating, confirming that the same spectral regions dominate the transition in both directions.

Overall, the majority of the spectral changes observed in the MFR data during heating of hydrated PNVCL were similar to those discussed for PNVCL powder, suggesting that temper-

https://doi.org/10.1021/acsapm.6c02142
ACS Appl. Polym. Mater. XXXX, XXX, XXX−XXX

ature-dependent changes in C═O bonding to water remain a key driver of the structural transition. In addition to these shared features, an additional spectral contribution was observed for hydrated PNVCL in the region around ∼1350 cm^{-1}. While this Raman shift has not previously been specifically assigned for PNVCL, bands in this frequency range are commonly associated with CH_2 vibrations, such as wagging or twisting modes.[40] In the case of PNVCL, these CH_2 groups are present both in the caprolactam ring and along the C−C polymer backbone. The increased contribution of the ∼1350 cm^{-1} region above the LCST may therefore reflect structural rearrangements within the polymer, including increased chain packing during the coil-to-globule transition. As the polymer chains collapse into a more compact conformation in aqueous solution, the local environment of CH_2 groups becomes more constrained and ordered, which could increase Raman scattering in this region. Alternatively, aggregation of PNVCL upon heating above the LCST has been reported[41,42] and may also contribute to the observed spectral changes. This interpretation is further supported by the LFR analysis, which directly probes collective and interchain dynamics (Supporting Information, Figure S6C,E). Although heating and cooling involve the same spectral regions, the PC1 scores plots (Figure 6D,F) are not identical, indicating that the structural pathway followed upon cooling is not a simple reversal of the heating process. This suggests that folding and unfolding of hydrated PNVCL do not occur in the same manner and that the polymer may not fully return to an identical structural state after thermal cycling.

Taken together, comparison of PNVCL powder and hydrated PNVCL demonstrates that thermoresponsive behavior is retained across hydration states, although the magnitude and spectral manifestation of the transition depend strongly on the water content. In powder, the structural transition is less pronounced, indicating that limited hydration constrains polymer mobility and suppresses contributions from CH_2−related motions, while changes in C═O interactions with residual water remain detectable. In contrast, hydration enables additional intramolecular and intermolecular rearrangements consistent with a more complete coil-to-globule transition. These experimental observations are in good agreement with molecular dynamics simulations by Zhelavskyi and Kyrychenko,[38] which demonstrated a pronounced difference in the hydration state of the carbonyl group of PNVCL below and above the LCST. Subsequently, Camara et al.[39] identified the carbonyl group (C═O) as the primary and effectively the only functional group in PNVCL capable of forming hydrogen bonds with surrounding water molecules. The shift of the structural transition to lower temperatures for less hydrated PNVCL further aligns with the established concentration dependence of the LCST (Figure 5), where higher effective polymer concentrations result in lower transition temperatures.

3.3.4. SAXS/WAXS Reveal Size Increase Followed by Decrease when Heating above the LCST. To extend the molecular insights obtained from Raman spectroscopy to larger structural length scales, SAXS and WAXS serve as powerful complementary techniques. SAXS provides information on polymer conformation and aggregation on the nanometer scale, while WAXS is sensitive to short-range order and crystallinity. To the best of our knowledge, this is the first temperature-resolved SAXS/WAXS study published for PNVCL, although similar analyses exist for PNIPAM.[43] PNVCL was investigated in hydrated (1000 mg/mL) and dissolved (100 mg/mL) states during heating from 20 to 50 °C (Figure 7) and subsequent cooling from 50 to 20 °C (Supporting Information, Figure S8). The SAXS data were fitted using a unified fit model[25] extracting the radius of gyration (R_g) from each scattering curve (Figure 7). Examples of fits are provided (Supporting Information, Figure S9).

Across all conditions, SAXS and WAXS revealed continuous, temperature-dependent structural rearrangements through variations in scattering intensity and curve profile during heating (Figure 7) and subsequent cooling (Supporting Information, Figure S8). SAXS data were fitted to extract a radius of gyration (R_g) at each temperature during heating and cooling (Figure 7G). As PNVCL undergoes conformational changes with temperature, a unified Beaucage-derived model was chosen for the fit, offering reasonable approximation of scattering from multiple structures, including coils and clusters.[25] Examples of fits (Supporting Information, Figure S9) display reasonable fits with minor low-q underestimation for some dissolved samples. WAXS data consistently indicated an amorphous structure, in agreement with XRPD patterns (Supporting Information, Figure S5B). While other XRPD reports for PNVCL confirm an overall amorphous nature with additional indication of paracrystalline ordering,[26,27] no such ordering was detected here, likely explained by the low molecular weight of the synthesized PNVCL.

For hydrated PNVCL, the SAXS data obtained during heating (Figure 7A) revealed an increase in scattering intensity up to 39 °C, followed by a decrease, most evident in the low-q region. The WAXS data (Figure 7B) displayed a similar trend. During cooling the behavior reversed (Supporting Information, Figure S8A,B). Fitted SAXS data (Figure 7G) revealed a size increase until reaching a maximum R_g at 40 °C during heating and 37 °C during cooling, followed by a decrease in size. For dissolved PNVCL, similar trends were observed during heating (Figure 7C,D) and cooling (Supporting Information, Figure S8C,D). The maximum scattering intensity was reached at 36 °C for dissolved PNVCL during heating, while fitted SAXS data (Figure 7G) displayed a maximum R_g at 36 °C during heating and 34 °C during cooling. The increase in low-q scattering intensity below the LCST suggests structure growth, driven by partial dehydration and interchain attraction that produce larger effective scattering objects in terms of early stage aggregates. The subsequent decline above the LCST likely reflects (i) a decrease in apparent size and (ii) a loss of scattering objects, consistent with the collapse of PNVCL and the continuous aggregation, driving precipitation of larger PNVCL aggregates and leaving only smaller, still soluble aggregates in the beam. Considering also that R_g is unaffected by the scattering intensity variations, it is more likely that the precipitation of larger PNVCL aggregates is what is causing the observed drastic decrease in R_g above the LCST; a process that is driven by the collapse of PNVCL. Temperature-resolved SAXS/WAXS for the thermoresponsive polymer PNIPAM has shown a similar decline in scattering intensity above the LCST due to precipitation.[43]

Kratky plots were introduced to distinguish flexible, coil-like structures and compact, globular structures at temperatures below, around and above the LCST. At 20 °C, the rising slope reflects an extended, coil-like conformation. At 39 °C, a bell-shaped feature emerged in the low-q region, together with a decrease in slope, indicating a transition toward more compact structures, characteristic of globule formation. Dissolved PNVCL displayed an even stronger compact signature than

https://doi.org/10.1021/acsapm.6c02142
ACS Appl. Polym. Mater. XXXX, XXX, XXX−XXX

hydrated PNVCL, reflecting enhanced water interactions, greater chain mobility, and a more pronounced coil-to-globule transition, consistent with Raman spectroscopy findings. At 50 °C, the Kratky curve flattened and the bell-shaped feature diminished. Rather than indicating a return to an extended conformation, this loss of structure is most likely due to the reduced scattering intensity resulting from collapse and precipitation of PNVCL, affecting the background subtraction and masking characteristic Kratky features.

Comparison of heating and cooling (Figure 7G) indicated partially reversible thermoresponsive behavior, consistent with Raman data. SAXS confirmed rapid folding during heating but slower unfolding during cooling as well as slight variations between the starting point of heating and the end point of cooling, suggesting that PNVCL adopts a slightly different structure following a heating−cooling cycle. As for Raman data, these discrepancies are likely a consequence of hysteresis arising from persistent aggregates or incomplete hydration slowing down the unfolding process. The hydration-dependence of the cooling behavior supports this interpretation, as persistent aggregates in hydrated PNVCL raise the cooling peak, while rapid rehydration in dissolved PNVCL lowers it.

In terms of PNVCL size, Dittrich et al.[29] used molecular dynamics simulation to estimate the R_g of a single, fully extended 40mer PNVCL chain, obtaining a size of 25 Å. This is in agreement with estimations from the fitted SAXS data (Figure 7G). PNVCL synthesized in this study consists of 5−35mers, making it reasonably comparable in size to the 40mer studied by Dittrich et al.[29] Camara et al.[39] applied molecular dynamics simulations to study PNVCL under temperature-resolved conditions. End-to-end distance of the PNVCL backbone was estimated as 33 Å at temperatures below the LCST and 25 Å above the LCST, which is comparable to the size range obtained in our study from SAXS data fitting (Figure 7G). However, the authors' simulations showed size consistency above and below the LCST,[39] which does not match the SAXS trend of increasing size up until the LCST followed by a decrease that we observed. The discrepancy is likely due to their model considering only a single, non-interacting PNVCL chain,[39] thereby not accounting for any aggregation and precipitation effects detected by SAXS. This highlights the importance of obtaining experimental temperature-resolved data for PNVCL.

Across all complementary characterization techniques, SAXS and WAXS (Figure 7) displayed continuous structural rearrangements of PNVCL, while both UV−vis spectrophotometry (Figure 5) and Raman spectroscopy (Figure 6) probed distinct and rapid changes, occurring at a temperature corresponding to the LCST. This explains the slight inconsistencies in the LCSTs determined by the different methods, which probe structural transitions occurring at different length scales. For dissolved PNVCL, the peak in SAXS intensity occurred at 36 °C (Figure 7C), while the LCST was determined to be 39 ± 1 °C using UV−vis spectrophotometry (Figure 5), suggesting that SAXS detects conformational changes occurring prior to the UV-detectable precipitation of PNVCL. For hydrated PNVCL, the scattering intensity was highest at 39 °C (Figure 7A). Using Raman spectroscopy, the structural transition was detected at 38 °C, suggesting that the temperature-dependent reorganization is represented similarly across the different length scales probed by Raman spectroscopy and SAXS. Considering the continuous alteration of PNVCL structure observed with SAXS/WAXS throughout heating and cooling, alongside the findings of PNVCL continuously aggregating with further heating above the LCST, the results suggest that it not only matters whether PNVCL is utilized for drug delivery purposes above or below the LCST, but also how far the physiological temperature is from the LCST in either direction.

4. CONCLUSIONS

In this work, we addressed key limitations hindering the broader adoption of PNVCL for stimuli-responsive drug delivery. By providing optimization data for free radical polymerization and applying a multimethod approach for molecular weight estimation, this work guides improved reproducibility and standardization in PNVCL research. The molecular weight of the synthesized PNVCL was characterized by GPC, osmometry, MALDI-MS, and DOSY-NMR, yielding a low molecular weight <5000 g/mol and a dispersity in the range of 1.2−1.8.

Complementary techniques, including UV−vis spectrophotometry, SAXS/WAXS, and Raman spectroscopy, were employed to demonstrate that PNVCL undergoes hydration-dependent structural transitions consistent with a coil-to-globule transition around the LCST, followed by aggregation at higher temperatures. Further, correlating changes across multiple length scales revealed that the thermoresponsive behavior is retained across all hydration states, although the magnitude and spectral manifestation of the transition depend strongly on the water content. A key finding is that the thermoresponsive behavior is not restricted to the dissolved form of PNVCL predominantly studied in literature, highlighting its potential for temperature-responsive drug delivery applications at a wide hydration range.

This study also highlights how subtle variations in polymer concentration introduce LCST shifts of several degrees. Structural transitions were observed by Raman spectroscopy at 27 °C for powder PNVCL and by UV−vis spectroscopy at 48 °C for highly diluted PNVCL (10 mg/mL in water), spanning from below to above physiologically relevant temperatures. As the PNVCL concentration inevitably changes upon administration, when the vehicle evaporates or mixes with biological fluids, the LCST must be reassessed under application-specific conditions to ensure maintenance of temperature responsiveness in the physiological environment. Given that additional factors such as solvent composition and salt concentration also influence LCST, future studies should extend this multimethod approach to more complex solvents. The findings presented here are based on several batches of PNVCL prepared to obtain a single low molecular weight polymer, and the observed trends therefore apply specifically to this system and should be expanded to include higher molecular weight PNVCL polymers and more complex PNVCL-based systems, to allow for investigation of the impact of molecular weight and organization.

Raman signatures of carbonyl hydration and CH_2−related chain organization, together with SAXS-derived measures of compaction and aggregation, could serve as complementary descriptors for the rational screening and computational design of PNVCL-based systems. Future studies should assess their stability during storage, thermal cycling, and exposure to physiologically relevant media, followed by drug-release, biocompatibility, and in vivo evaluation under relevant dilution conditions. From a sustainability perspective, Raman spectroscopy and SAXS/WAXS are largely nondestructive, require

https://doi.org/10.1021/acsapm.6c02142
ACS Appl. Polym. Mater. XXXX, XXX, XXX−XXX

small sample quantities, and minimize solvent and reagent use. However, they rely on specialized instrumentation and can be resource-intensive in terms of instrument time, energy use, and infrastructure, emphasizing the value of efficient experimental design and tiered screening strategies.

■ ASSOCIATED CONTENT

Supporting Information

The Supporting Information is available free of charge at https://pubs.acs.org/doi/10.1021/acsapm.6c02142.

Additional ^{1}H NMR spectra for free radical polymerization optimization and comparison to commercial PNVCL; TGA thermogram; XRPD pattern; Raman (LFR) spectra; Raman PC1 loadings plots; SAXS/WAXS cooling data; fitted SAXS curves; GPC chromatograms; LCST derivative analysis (PDF)

■ AUTHOR INFORMATION

Corresponding Author

Hanne Mørck Nielsen − *Center for Biopharmaceuticals and Biobarriers in Drug Delivery (BioDelivery), Department of Pharmacy, Faculty of Health and Medical Sciences, University of Copenhagen, 2100 Copenhagen, Denmark;* orcid.org/0000-0002-7285-9100; Email: hanne.morck@sund.ku.dk

Authors

Camilla Hald Gregersen − *Center for Biopharmaceuticals and Biobarriers in Drug Delivery (BioDelivery), Department of Pharmacy, Faculty of Health and Medical Sciences, University of Copenhagen, 2100 Copenhagen, Denmark; LEO Foundation Center for Cutaneous Drug Delivery, Department of Pharmacy, Faculty of Health and Medical Sciences, University of Copenhagen, 2100 Copenhagen, Denmark;* orcid.org/0000-0002-4533-7710

Kārlis Bērziņš − *Center for Pharmaceutical Data Science Education (CPDSE), Department of Pharmacy, Faculty of Health and Medical Sciences, University of Copenhagen, 2100 Copenhagen, Denmark;* orcid.org/0000-0001-6545-5522

Jacob Judas Kain Kirkensgaard − *Department of Food Science, University of Copenhagen, 1958 Frederiksberg C, Denmark; Niels Bohr Institute, University of Copenhagen, 2100 Copenhagen, Denmark;* orcid.org/0000-0001-6265-0314

Işık Perçin Demirçelik − *Center for Biopharmaceuticals and Biobarriers in Drug Delivery (BioDelivery), Department of Pharmacy, Faculty of Health and Medical Sciences, University of Copenhagen, 2100 Copenhagen, Denmark; Department of Biology, Hacettepe University, 06800 Ankara, Turkey*

Charalampos Sideris − *Department of Health Technology, Technical University of Denmark, 2800 Lyngby, Denmark;* orcid.org/0009-0004-4352-0281

Ben J. Boyd − *Drug Delivery, Disposition and Dynamics, Monash Institute of Pharmaceutical Sciences, Parkville, Victoria 3052, Australia; Department of Pharmacy, University of Copenhagen, 2100 Copenhagen, Denmark;* orcid.org/0000-0001-5434-590X

Jørn Bolstad Christensen − *Department of Chemistry, University of Copenhagen, 1871 Frederiksberg C, Denmark;* orcid.org/0000-0002-7641-8302

Andrea Heinz − *LEO Foundation Center for Cutaneous Drug Delivery, Department of Pharmacy, Faculty of Health and Medical Sciences, University of Copenhagen, 2100 Copenhagen, Denmark;* orcid.org/0000-0002-8609-4460

Complete contact information is available at: https://pubs.acs.org/10.1021/acsapm.6c02142

Funding

The work was financially supported by the LEO Foundation (grant no. LF-ST-21-500005 (H.M.N.), grant no. LF15007 (A.H.), and grant no. LF-ST-24-500013 (K.B.)); the Novo Nordisk Foundation (grant no. NNF16OC0021948 (H.M.N.) through funding to the Center for Biopharmaceuticals and Biobarriers in Drug Delivery, grant no. NNF24SA0092613 (K.B.), and grant no. NNF20OC0059614 (B.J.B. and K.B. as part of B.J.B.'s Novo Nordisk Foundation Laureate Research Fellowship); the Lundbeck Foundation (grant no. R469-2024-629 (K.B.) through funding to the Center for Pharmaceutical Data Science Education); the Danish Agency for Higher Education and Science (grant no. 726510 (J.J.K.K.) through funding to the ESS Lighthouse: Colloids and Interfaces in Food and Pharma); and the Scientific and Technological Research Council of Turkey (TÜBİTAK) for the postdoctoral research fellowship granted under the 2219-program (2023−2024) (I.P.D). X-ray scattering data were produced by the research infrastructure at The Department of Food Science at the University of Copenhagen, partly funded by FOODHAY (Food and Health Open Innovation Laboratory, Danish Roadmap for Research Infrastructure). The authors thank the Villum Foundation (grant no. 19175) for funding the CLARIOstar plate reader. The funding sources have not been involved in the study design or in writing this publication.

Notes

The authors declare no competing financial interest.

■ ABBREVIATIONS

AIBN, 2,2-azobis(isobutyronitrile); ATRP, atom transfer radical polymerization; CDCl3, chloroform-D1; DCM, dichloromethane; DHB, dihydroxybenzoic acid; DMF, *N,N*-dimethylformamide; DOSY, diffusion-ordered spectroscopy; GPC, gel permeation chromatography; HO-TEMPO, 4-hydroxy-2,2,6,6-tetramethylpiperidine-1-oxyl; HPLC, high-performance liquid chromatography; LCST, lower critical solution temperature; LFR, low-frequency Raman; MALDI-MS, matrix-assisted laser desorption ionization mass spectrometry; MFR, midfrequency Raman; M_n, number-average molecular weight; M_v, viscosity-average molecular weight; M_w, weight-average molecular weight; n_B, batch replicates; NMR, nuclear magnetic resonance; n_t, technical replicates; NVCL, *N*-vinylcaprolactam; PC, principal component; PCA, principal component analysis; PEG, polyethylene glycol; PHPA, poly(2-hydroxypropyl acrylate); PMAA, poly(methacrylic acid); PNIPAM, poly(*N*-isopropylacrylamide); PNVCL, poly(*N*-vinylcaprolactam); PTFE, polytetrafluoroethylene; RAFT, reversible addition−fragmentation chain transfer; R_g, radius of gyration; R_h, hydrodynamic radius; SAXS, small-angle X-ray scattering; SD, standard deviation; SEM, scanning electron microscopy; SNV, standard normal variate; TGA, thermogravimetric analysis; THF, tetrahydrofuran; UV−vis, ultraviolet−visible; WAXS, wide-angle X-ray scattering; XRPD, X-ray powder diffraction.

REFERENCES

(1) Mura, S.; Nicolas, J.; Couvreur, P. Stimuli-responsive nanocarriers for drug delivery. *Nat. Mater.* **2013**, *12* (11), 991−1003.

(2) Karimi, M.; Sahandi Zangabad, P.; Ghasemi, A.; Amiri, M.; Bahrami, M.; Malekzad, H.; Ghahramanzadeh Asl, H.; Mahdieh, Z.; Bozorgomid, M.; Ghasemi, A.; et al. Temperature-responsive smart nanocarriers for delivery of therapeutic agents: Applications and recent advances. *ACS Appl. Mater. Interfaces* **2016**, *8* (33), 21107−21133.

(3) Ribeiro, T. P.; Gomes, F. L.; Vilarinho, R.; Salgado, C.; Martins, M. C. L.; Moreira, J. A.; Monteiro, F. J.; Laranjeira, M. S. Thermoresponsive nanoparticles for targeted and controlled delivery of doxorubicin in triple negative breast cancer: a 2D and 3D in vitro evaluation. *Drug Delivery Transl. Res.* **2026**, *16* (1), 108−123.

(4) BASF. *Technical information for Luviskol® Plus from BASF*, 2005. https://cdn.vanderbilt.edu/vu-wpfsx/wp-content/uploads/sites/40/2024/03/09202731/Luviskol_plus.pdf (accessed 09.05.2026).

(5) Sefidroodi, H.; Cheng Chua, P.; Kelland, M. A. THF hydrate crystal growth inhibition with small anionic organic compounds and their synergistic properties with the kinetic hydrate inhibitor poly(N-vinylcaprolactam). *Chem. Eng. Sci.* **2011**, *66* (10), 2050−2056.

(6) Liu, J.; Debuigne, A.; Detrembleur, C.; Jerome, C. Poly(N-vinylcaprolactam): A thermoresponsive macromolecule with promising future in biomedical field. *Adv. Healthcare Mater.* **2014**, *3* (12), 1941−1968.

(7) Cortez-Lemus, N. A.; Licea-Claverie, A. Poly(N-vinylcaprolactam), a comprehensive review on a thermoresponsive polymer becoming popular. *Prog. Polym. Sci.* **2016**, *53*, 1−51.

(8) Halligan, S. C.; Dalton, M. B.; Murray, K. A.; Dong, Y.; Wang, W.; Lyons, J. G.; Geever, L. M. Synthesis, characterisation and phase transition behaviour of temperature-responsive physically crosslinked poly (N-vinylcaprolactam) based polymers for biomedical applications. *Mater. Sci. Eng., C* **2017**, *79*, 130−139.

(9) Medeiros, S. F.; Barboza, J. C. S.; Ré, M. I.; Giudici, R.; Santos, A. M. Solution polymerization of N-vinylcaprolactam in 1,4-dioxane. Kinetic dependence on temperature, monomer, and initiator concentrations. *J. Appl. Polym. Sci.* **2010**, *118* (1), 229−240.

(10) Marsili, L.; Dal Bo, M.; Eisele, G.; Donati, I.; Berti, F.; Toffoli, G. Characterization of thermoresponsive poly-N-vinylcaprolactam polymers for biological applications. *Polym.* **2021**, *13* (16), 2639.

(11) Meeussen, F.; Nies, E.; Berghmans, H.; Verbrugghe, S.; Goethals, E.; Du Prez, F. Phase behaviour of poly(N-vinyl caprolactam) in water. *Polym.* **2000**, *41* (24), 8597−8602.

(12) LauWu, A. C. W. C. Thermally sensitive and biocompatible poly(N-vinylcaprolactam): Synthesis and characterization of high molar mass linear chains. *Macromol.* **1999**, *32* (3), 581.

(13) Vihola, H.; Laukkanen, A.; Valtola, L.; Tenhu, H.; Hirvonen, J. Cytotoxicity of thermosensitive polymers poly(N-isopropylacrylamide), poly(N-vinylcaprolactam) and amphiphilically modified poly-(N-vinylcaprolactam). *Biomaterials* **2005**, *26* (16), 3055−3064.

(14) Liu, L.; Bai, S.; Yang, H.; Li, S.; Quan, J.; Zhu, L.; Nie, H. Controlled release from thermo-sensitive PNVCL-co-MAA electrospun nanofibers: The effects of hydrophilicity/hydrophobicity of a drug. *Mater. Sci. Eng., C* **2016**, *67*, 581−589.

(15) Pünnel, L. C.; Lunter, D. J. Film-forming systems for dermal drug delivery. *Pharmaceutics* **2021**, *13* (7), 932.

(16) Sta, M.; Tada, D. B.; Medeiros, S. F.; Santos, A. M.; Demarquette, N. R. Hydrophilic drug release from electrospun membranes made out of thermo and pH-sensitive polymers. *J. Drug Delivery Sci. Technol.* **2022**, *71*, 103284.

(17) Sta, M.; Aguiar, G.; Forni, A. A. J.; Medeiros, S. F.; Santos, A. M.; Demarquette, N. R. Design and characterization of PNVCL-based nanofibers and evaluation of their potential applications as scaffolds for surface drug delivery of hydrophobic drugs. *J. Appl. Polym. Sci.* **2020**, *137* (11), 48472.

(18) Marsili, L.; Dal Bo, M.; Berti, F.; Toffoli, G. Thermoresponsive chitosan-grafted-poly(N-vinylcaprolactam) microgels via ionotropic gelation for oncological applications. *Pharmaceutics* **2021**, *13* (10), 1654.

(19) Sala, R. L.; Kwon, M. Y.; Kim, M.; Gullbrand, S. E.; Henning, E. A.; Mauck, R. L.; Camargo, E. R.; Burdick, J. A. Thermosensitive poly(N-vinylcaprolactam) injectable hydrogels for cartilage tissue engineering. *Tissue Eng., Part A* **2017**, *23* (17−18), 935−945.

(20) Kumar, K.; Umapathi, R.; Bisht, M.; Ghoreishian, S. M.; Huh, Y. S.; Venkatesu, P. Tweaking behavior of hydrogen bond donor in choline chloride-based deep eutectic solvents for regulating the phase transition of Poly(N-vinylcaprolactam): A sustainable medium for an early hydrophobic collapse. *ACS Sustainable Chem. Eng.* **2021**, *9* (43), 14335−14344.

(21) Zhao, W.; Chen, J.; Zuo, H.; Jiao, Y.; Wang, F.; Du, W.; Sai, F.; Tong, S.; Li, Y. Development of P(NVCL)-based transdermal patches for sinomenine hydrochloride delivery in gouty arthritis. *Colloids Surf., B* **2025**, *256*, 115055.

(22) Fatriyah, S.; Nizardo, N. M.; Saputri, F. C.; Jung, H.; Lee, A.; Mulyadi, C. A.; Willie, Y. B. A.; Marwah, M.; Ramadon, D. Development of poly(vinyl alcohol)/poly(N-vinyl caprolactam)-based hydrogel-forming microneedle for transdermal delivery of captopril: fabrication, characterization and in vivo antihypertensive activity test. *Drug Delivery Transl. Res.* **2026**.

(23) Bordat, A.; Boissenot, T.; Nicolas, J.; Tsapis, N. Thermoresponsive polymer nanocarriers for biomedical applications. *Adv. Drug Delivery Rev.* **2019**, *138*, 167−192.

(24) Bērziņš, K.; Meiland, P.; Aljabbari, A.; Boyd, B. J. In operando analysis of milk-based oral formulations during digestion using synchrotron small-angle X-ray scattering coupled to low-frequency Raman spectroscopy. *Anal. Chem.* **2024**, *96* (2), 887−894.

(25) SasView. *SasView: Unified Power Rg Model*, 2026. https://www.sasview.org/docs/user/models/unified_power_Rg.html (accessed 26.11.2025).

(26) Kozanoğlu, S.; Özdemir, T.; Usanmaz, A. Polymerization of N-vinylcaprolactam and characterization of poly(N-vinylcaprolactam). *J. Macromol. Sci., Part A* **2011**, *48* (6), 467−477.

(27) Marimuthu, E.; Murugesan, V. Polymerization of N-vinyl caprolactam by ultrasound aided dual-sited phase transfer catalytic conditions. *Adv. Compos. Hybrid Mater.* **2019**, *2* (4), 670−680.

(28) Sun, S.; Wu, P. Infrared spectroscopic insight into hydration behavior of poly(N-vinylcaprolactam) in water. *J. Phys. Chem. B* **2011**, *115* (40), 11609−11618.

(29) Dittrich, J.; Kather, M.; Holzberger, A.; Pich, A.; Gohlke, H. Cumulative submillisecond all-atom simulations of the temperature-induced coil-to-globule transition of poly(N-vinylcaprolactam) in aqueous solution. *Macromol.* **2020**, *53* (22), 9793−9810.

(30) Su, W.-F. *Principles of Polymer Design and Synthesis*; Springer Berlin, 2013. ISBN: 978−3-642−38730−2.

(31) Nakamura, Y.; Terao, K.; Hirano, T.; Takano, A. *Characterization of Polymers in Solution: Experimental Determination of Molecular Parameters*; Springer Singapore, 2025. ISBN: 978−981−96−6677−5.

(32) Jiang, X.; Li, Y.; Lu, G.; Huang, X. A novel poly(N-vinylcaprolactam)-based well-defined amphiphilic graft copolymer synthesized by successive RAFT and ATRP. *Polym. Chem.* **2013**, *4* (5), 1402−1411.

(33) Zhao, Z.; Yin, L.; Yuan, G.; Wang, L. Layer-by-layer assembly of two temperature-responsive homopolymers at neutral pH and the temperature-dependent solubility of the multilayer film. *Langmuir* **2012**, *28* (5), 2704−2709.

(34) Kharlampieva, E.; Kozlovskaya, V.; Tyutina, J.; Sukhishvili, S. A. Hydrogen-bonded multilayers of thermoresponsive polymers. *Macromol.* **2005**, *38*, 10523−10531.

(35) Lee, B.; Jiao, A.; Yu, S.; You, J. B.; Kim, D. H.; Im, S. G. Initiated chemical vapor deposition of thermoresponsive poly(N-vinylcaprolactam) thin films for cell sheet engineering. *Acta Biomater.* **2013**, *9* (8), 7691−7698.

(36) Assis, J. F.; Gabriel, A. M.; Gonçalves, L. F.; Machado, M. R. F.; Morgado, D. L.; Sala, R. L.; Cristovan, F. H.; Oliveira, M. P.; Arantes, T. M.; Camargo, E. R. Thermosensitive and biocompatible nanocomposites of poly(N-vinylcaprolactam) and hydroxyapatite with potential use for bone tissue repair. *BioNanoScience* **2022**, *12* (3), 766−773.

(37) Kontoyannis, C. G.; Bouropoulos, N. C.; Koutsoukos, P. G. Quantitative analysis of impurities in Îμ-caprolactam by Raman spectroscopy. *Analyst* **1995**, *120* (2), 347−350.
(38) Zhelavskyi, O. S.; Kyrychenko, A. Atomistic molecular dynamics simulations of the LCST conformational transition in poly(N-vinylcaprolactam) in water. *J. Mol. Graph. Model.* **2019**, *90*, 51−58.
(39) Camara, M.; Xu, J.; Ding, T.; Zhou, W.; Sun, J.; Liao, H.; Zhang, J. Molecular dynamics study of the thermosensitive properties of poly (N-vinyl caprolactam) in water. *Fluid Phase Equilib.* **2021**, *527*, 112831.
(40) Brown, J. K.; Sheppard, N.; Simpson, D. M. The interpretation of the infra-red and Raman spectra of the n-paraffins. *Philos. Trans. R. Soc. London, Ser. A* **1954**, *247* (922), 35−58.
(41) Aseyev, V.; Hietala, S.; Laukkanen, A.; Nuopponen, M.; Confortini, O.; Du Prez, F. E.; Tenhu, H. Mesoglobules of thermoresponsive polymers in dilute aqueous solutions above the LCST. *Polymer* **2005**, *46* (18), 7118−7131.
(42) Chee, C. K.; Rimmer, S.; Soutar, I.; Swanson, L. Fluorescence investigations of the conformational behaviour of poly(N-vinyl-caprolactam). *React. Funct. Polym.* **2006**, *66*, 1−11.
(43) Lyngsø, J.; Al-Manasir, N.; Behrens, M. A.; Zhu, K.; Kjøniksen, A.-L.; Nyström, B.; Pedersen, J. S. Small-angle X-ray scattering studies of thermoresponsive poly(N-isopropylacrylamide) star polymers in water. *Macromol.* **2015**, *48* (7), 2235−2243.

https://doi.org/10.1021/acsapm.6c02142
ACS Appl. Polym. Mater. XXXX, XXX, XXX−XXX